

J.E. MEDVEDEVA

Unconventional approaches to combine optical transparency with electrical conductivity

Department of Physics, University of Missouri, Rolla, MO 65409, USA

Received: 10 October 2006/Accepted: 5 April 2007
Published online: 13 June 2007 • © Springer-Verlag 2007

ABSTRACT The combination of electrical conductivity and optical transparency in the same material – known to be a prerogative of only a few oxides of post-transition metals, such as In, Sn, Zn and Cd – manifests itself in a distinctive band structure of the transparent conductor host. While the oxides of other elements with s^2 electronic configuration, for example, Mg, Ca, Sc and Al, also exhibit the desired optical and electronic features, they have not been considered as candidates for achieving good electrical conductivity because of the challenges of efficient carrier generation in these wide-bandgap materials. Here we demonstrate that alternative approaches to the problem not only allow for attaining the transport and optical properties which compete with those in currently utilized transparent conducting oxides (TCO), but also significantly broaden the range of materials with a potential of being developed into novel functional transparent conductors.

PACS 71.20.-b; 72.20.-i

The key attribute of any conventional n-type TCO host is a highly dispersed single free-electron-like conduction band [1–8]. Upon proper doping, it provides both (1) high mobility of extra carriers (electrons) due to their small effective mass, and (2) low optical absorption in the visible part of the spectrum due to high-energy interband transitions (see Fig. 1). For the complete transparency in the visible range, the transitions from the valence band, E_v , and from the partially filled conduction band, E_c , should be larger than 3.1 eV, while the intraband transitions as well as the plasma frequency should be smaller than 1.8 eV. The high energy dispersion also ensures a pronounced Fermi energy displacement, the so-called Burstein–Moss (BM) shift, so that the optical transparency can be achieved in a material with a relatively small bandgap, for example, in CdO where the optical (direct) bandgap is 2.3 eV.

Figures 1a, b illustrate the typical conduction band of a conventional n-type transparent conductor and how doping alters the electronic band structure of the TCO host affecting the optical transitions. It is seen that upon introduction of extra carriers into the host, a large BM shift

which facilitates higher-energy transitions from the valence band (E_v), leads to a reduced energy of the transitions from the Fermi level up into the conduction band (E_c), i.e., E_v and E_c are interconnected.¹ In other words, large carrier concentrations desired for good conductivity, may result in an increase of the optical absorption because the E_c transitions become smaller in energy. In addition, the transitions within the partially filled band as well as plasma frequency may lead to the absorption in the long-wavelength range.

The mutual exclusiveness of the optical transmittance and electrical conductivity (see also [5, 9, 10]) makes it challenging to achieve the optimal performance in a transparent conductor. Below we outline novel, unconventional ways to balance the optical and transport properties and to improve one without making a sacrifice of the other.

1 Magnetically mediated transparent conductors

One of the possible routes to avoid compromising the optical transparency is to enhance conductivity via mobility of the carriers rather than their concentration [10]. Recently, the mobility with more than twice the value of the commercial Sn-doped indium oxide (ITO) was observed in Mo-doped In_2O_3 (IMO), and it was shown that the conductivity can be significantly increased with no changes in the spectral transmittance upon doping with Mo [11–14]. Surprisingly, the introduction of the transition metal Mo, which donates two more carriers per substitution compared to Sn, does not lead to the expected increase of the optical absorption or a decrease of the mobility due to the scattering on the localized Mo d -states.

Our electronic band structure investigations of IMO revealed [8] that the magnetic interactions which have never been considered to play a role in combining optical transparency with electrical conductivity, ensure both high carrier mobility and low optical absorption in the visible range. As one can see from Figs. 1c, d, strong exchange interactions split the Mo d -states located in the vicinity of the Fermi level.

¹ We note that in Sn-doped In_2O_3 (ITO) the second, or so-called hybridization gap which was argued to be one of the reasons of low optical absorption in ITO [1, 2] closes upon structural relaxation, i.e., when the Sn-O and In-O distances are optimized.

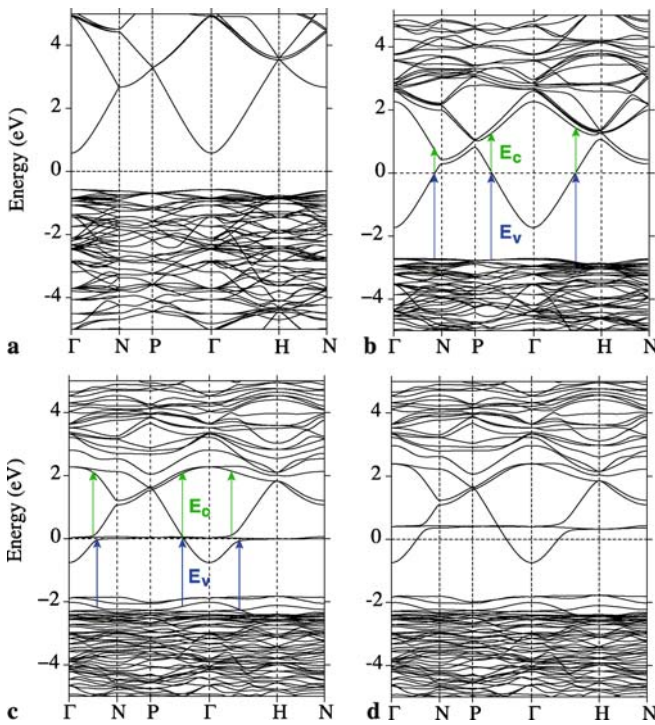


FIGURE 1 Electronic band structure of pure (a), 6.25% Sn-doped (b), and 6.25% Mo-doped In_2O_3 for the majority (c) and the minority (d) spin channels

These d -states are resonant states, while the conductivity is due to the delocalized In s -states, which form the highly dispersed free-electron-like conduction band. In other words, the free carriers in the system flow in a background of the Mo defects, which serve as strong scattering centers. Because of the exchange splitting of the Mo d -states, the carriers of one spin are affected by only half the scattering centers, i.e., only by the Mo d -states of the same spin. Therefore, the concentration of the Mo scattering centers is effectively lowered by a half compared to the Mo doping level.

Figures 1b–d show that the BM shift is less pronounced in the IMO case – despite the fact that Mo^{6+} donates two extra carriers as compared to Sn^{4+} at the same doping level. Such a low sensitivity to doping appears from the resonant Mo d -states located at the Fermi level that facilitates the d -band filling (pinning) and thus hinders further displacement of the Fermi level deep into the conduction band. Smaller BM shifts in IMO lead to the following advantageous features, compared to those of ITO:

1. Smaller increase in the effective mass is expected upon Mo doping. In addition, the resonant Mo d -states do not hybridize with the s -states of indium and so do not affect the dispersion of the conduction band. Therefore, the effective mass remains similar to the one of pure indium oxide. This is borne out in experimental observations [13] showing that the effective mass does not vary with doping (up to 12% of Mo) and/or carrier concentration.
2. Larger (in energy) optical transitions from the partially occupied band (see Figs. 1b–d) along with the fact that transitions from d - to s -states are forbidden ensure lower short-wavelength optical absorption.

Complex	M	$E_g(0)$	$k_F^{[110]}$	$k_F^{[111]}$	$k_F^{[010]}$	ω_p
$\text{Mo}_{\text{In}(1)}^{\bullet\bullet}$	1.85	1.38	0.152	0.148	0.157	1.63
$\text{Mo}_{\text{In}(2)}^{\bullet\bullet}$	1.32	1.18	0.194	0.187	0.201	2.05
$[\text{Mo}_{\text{In}}^{\bullet\bullet}\text{O}_i^{\prime\prime}]^{\bullet}$	0.50	1.26	0.125	0.123	0.132	1.27
$\text{Sn}_{\text{In}(1)}^{\bullet}$	–	0.98	0.201	0.203	0.205	2.29
$\text{In}_2\text{O}_3 + e'$	–	1.16	0.206	0.204	0.213	2.38

TABLE 1 Calculated magnetic moments on the Mo atoms, M , in μ_B ; the fundamental band gap values $E_g(0)$, in eV; the Fermi wave vectors k_F , in atomic units; and the plasma frequency ω_p , in eV, for the different substitutional complexes with 6.25% Mo doping level. Calculated values for pure (rigid-band model) and 6.25% Sn-doped In_2O_3 are given for comparison

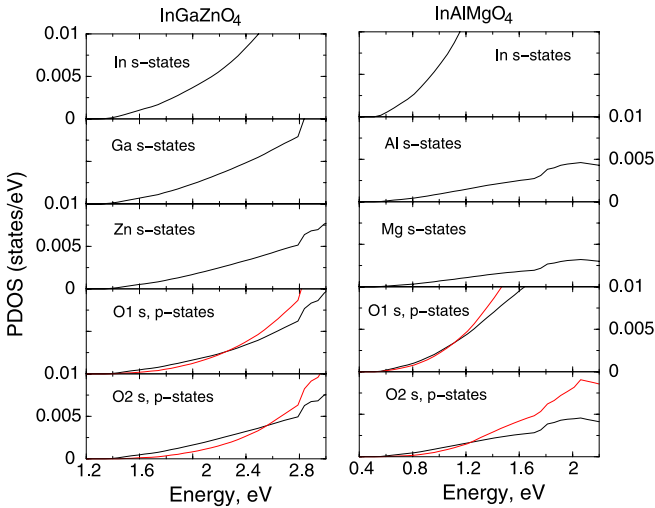
3. The calculated plasma frequency, ω_p , in IMO is below the visible range and significantly smaller than that of ITO (Table 1). This finding suggests a possibility to introduce larger carrier concentrations without sacrificing the optical transmittance in the long wavelength range.
4. Smaller BM shift does not lead to the appearance of the intense interband transitions from the valence band, E_v , in the visible range due to the large optical bandgap in pure indium oxide, namely, 3.6 eV [15]. Furthermore, in contrast to ITO where the bandgap narrowing has been demonstrated both experimentally [15] and theoretically [2], doping with Mo shows an opposite (beneficial) trend: the fundamental bandgap increases upon introduction of Mo (Table 1), because the asymmetric d -orbitals of Mo rotate the p -orbitals of the neighboring oxygen atoms leading to an increase of the overlap between the latter and the In s -states.

It is important to note that the optical and transport properties in IMO are sensitive to specific growth conditions, namely, the ambient oxygen pressure. It is found [8] that an increased oxygen content facilitates the formation of the oxygen compensated complexes, which reduces the number of free carriers – from 3 to 1 per Mo substitution – but, at the same time, improves the carrier mobility due to smaller ionized impurity scattering and hence longer relaxation times. On the other hand, the interstitial oxygen significantly suppresses the magnetic interactions (Table 1), which should be strong enough to split the transition metal d -states in order to provide good conductivity in one (or both) spin channels.

Thus, the transition metal dopants can be highly beneficial in providing the transport and optical properties which compete with those of commercially utilized ITO. Similar behavior is expected upon doping with other transition metal elements and other hosts, provided that the magnetic interactions are small enough to keep the d^\uparrow - d^\downarrow transitions out of the visible range.

2 Multicomponent TCO with layered structure

Complex transparent conductors consisting of structurally and/or chemically distinct layers, such as $\text{InGaO}_3(\text{ZnO})_m$, $m = \text{integer}$, offer a way to increase conductivity by spatially separating the carrier donors (traditionally, oxygen vacancies or aliovalent substitutional dopants) and conducting layers which transfer the carriers effectively, i.e., without charge scattering on the impurities [16–18].


 FIGURE 2 Partial density of states for InGaZnO₄ and InAlMgO₄

The homologous series InGaO₃(ZnO)_{*m*} and In₂O₃(ZnO)_{*m*}, also known for their promising thermoelectric properties [19], have been extensively studied experimentally [1, 17, 18, 20–24]. In these materials, octahedrally coordinated In layers alternate with (*m* + 1) layers of oxygen tetrahedrons around Zn (and Ga) [25–27]. Because the octahedral oxygen coordination of cations was long believed to be essential for a good transparent conductor [1, 4, 16, 28–31], it has been suggested that the charge is transferred within the InO_{1.5} layers while Ga and Zn atoms were proposed as candidates for efficient substitutional doping [1, 17, 18].

However, accurate electronic band structure investigations for InGaZnO₄, *m* = 1, showed [32] that the atoms from both InO_{1.5} and GaZnO_{2.5} layers give comparable contributions to the conduction band (Fig. 2a). This resulted in a three-dimensional distribution of the charge density calculated for the bottom of the conduction band: the interatomic (or “background”) electron density is similar in and across the [0001] layers. The isotropy of the electronic properties in this layered compound manifests itself in the electron effective masses being nearly the same in all crystallographic directions (Table 2).

Most strikingly, we found that the effective mass remains isotropic for multicomponent oxides of other metal elements with *s*² electronic configuration, for example, Sc, Al and/or Mg. This finding may seem to be counterintuitive, since the

s-states of Sc, Al and Mg are expected to be located deeper in the conduction band due to significantly larger bandgaps in Sc₂O₃, Al₂O₃ and MgO as compared to those in In₂O₃, Ga₂O₃ and ZnO. Analysis of the partial density of states shows that although the contributions from the Sc, Al and Mg atoms to the bottom of the conduction band are notably reduced (see Fig. 2 and Table 2), the states of these atoms are still available for the electron transport. Consequently, the interatomic charge density distribution is three-dimensional for all these layered multi-cation oxides – in accord with the isotropic electron effective mass. Moreover, we found [32] that the electron effective mass in these complex materials can be predicted via simple averaging over those of the corresponding single-cation oxides (Table 2).

It is important to stress that the isotropic character of the intrinsic transport properties in the TCO hosts with layered structure may not be maintained when extra carriers are introduced. Different valence states (e.g., In³⁺ and Ga³⁺ vs. Zn²⁺) and oxygen coordination (octahedral for In vs. tetrahedral for Ga and Zn) are likely to result in preferential (non-uniform) arrangement of aliovalent substitutional dopants or oxygen vacancies. We believe that the observed anisotropic conductivity [19, 20] as well as its dependence on the octahedral site density [1, 31] in the layered TCOs is a manifestation of a specific carrier generation mechanism. While proper doping can help make either or both structurally distinct layers conducting, leading to a highly anisotropic or three-dimensional electron mobility, respectively, amorphous complex oxides [21, 23, 24] readily offer a way to maintain isotropic transport properties.

Thus, we believe that other cations with *s*² electronic configuration, beyond the traditional In, Sn, Zn and Cd, can be effectively incorporated into novel complex multicomponent TCO hosts – such as the layered materials described above, ordered ternary oxides [31, 33–35], solid solutions [1] as well as their amorphous counterparts [21, 35], important for flexible electronics technologies [23]. Significantly, the sensitivity of the bandgap value to the composition of a multicomponent oxide (Table 2) offers a possibility to manipulate the optical properties as well as the band offsets (work functions) via proper composition of an application-specific TCO.

Finally, it should be mentioned, that the efficient doping of the wide-bandgap oxides is known to be a challenge [36–38]. Alternative carrier generation mechanisms, for example, magnetic dopants discussed above, introduction of hydrogen [39] or “free” ion targeting in nanoporous calcium aluminate [5, 40, 41], are being actively sought and have already yielded promising results – as outlined in the following section.

Compound	N ₁	N ₂	<i>E_g</i> (0)	<i>m</i> _[100]	<i>m</i> _[010]	<i>m</i> _[001]	<i>m_{ab}</i>	<i>m_z</i>
InGaZnO ₄	48%	52%	1.5	0.23	0.22	0.20	0.23	0.23
InAlCdO ₄	54%	46%	1.3	0.26	0.25	0.20	0.27	0.27
InGaMgO ₄	58%	42%	2.2	0.27	0.27	0.24	0.28	0.29
ScGaZnO ₄	26%	74%	2.5	0.33	0.33	0.34	0.33	0.53
InAlMgO ₄	72%	28%	2.8	0.32	0.31	0.35	0.31	0.34

TABLE 2 Net contributions to the conduction band at the *Γ* point from the states of the atoms that belong to the In(Sc)O_{1.5}, N₁, or Ga(Al)Zn(Cd, Mg)O_{2.5}, N₂, layers, in per cent; the LDA fundamental bandgap values *E_g*(0), in eV; the electron effective masses *m*, in *m_e*, along the specified crystallographic directions; and the components of the electron effective-mass tensor, *m_{a,b}* and *m_z*, calculated via simple averaging of those of the corresponding single-cation oxides

3 Novel transparent conductors: calcium aluminates

Case-structured insulating 12CaO · 7Al₂O₃, or mayenite, differs essentially from the conventional TCOs not only by its chemical and structural properties but also by the carrier generation mechanism: a persistent conductivity (with a ten-order of magnitude change) has been achieved upon doping with hydrogen followed by UV irradiation [40, 41].

Mayenite belongs to the CaO-Al₂O₃ family of Portland cements which are known for their superior refractory prop-

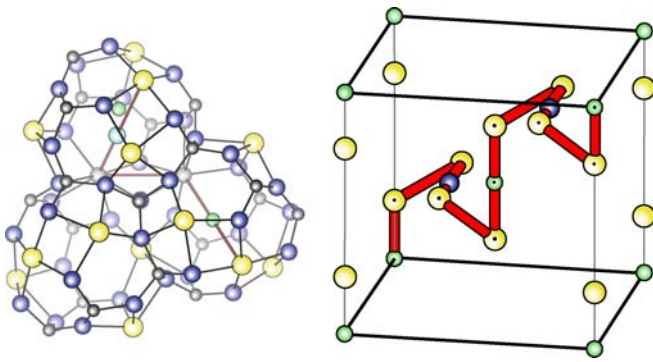


FIGURE 3 Crystal structure of H-doped $12\text{CaO} \cdot 7\text{Al}_2\text{O}_3$. On the left, only three of the 12 cages in the unit cell are shown. The cube (right) represent the unit cell. Only the atoms that participate in hopping transport are shown: Ca (yellow), OH^- (blue) and H^- (green spheres). Red line represents the electron hopping path

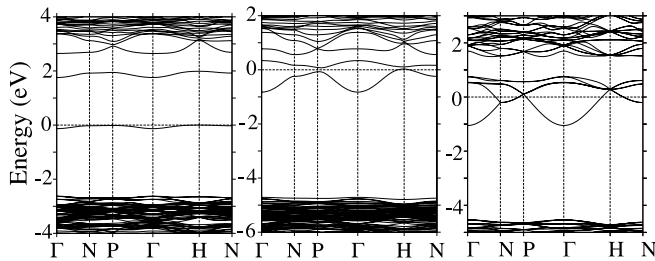


FIGURE 4 Electronic band structure of (a) H-doped and (b) H-doped UV-irradiated $\text{Ca}_{12}\text{Al}_{14}\text{O}_{33}$ and (c) $[\text{Ca}_{12}\text{Al}_{14}\text{O}_{32}]^{2+}(2e^-)$

erties. The unique structural features of mayenite (Fig. 3), namely, the engaged “excess” oxygen ions, allow incorporation of hydrogen according to the chemical reaction: $\text{O}^{2-}(\text{cage}) + \text{H}_2(\text{atm.}) \rightarrow \text{OH}^-(\text{cage}) + \text{H}^-(\text{another cage})$. While the H-doped mayenite remains insulating (Fig. 4a), the conductivity results from the electrons excited by UV irradiation off the H^- ions into the conduction band formed from Ca d -states. The charge transport occurs by electron hopping through the engaged “defects” – the H^0 and OH^- located inside the large (more than 5.6 \AA in diameter) structural cavities. Understanding of the conduction mechanism on the microscopic level [41, 42] resulted in prediction of ways to control the conductivity by targeting the particular atoms that participate in the hopping. These predictions have been confirmed experimentally [41, 43].

The low conductivity in H-doped UV-irradiated mayenite ($\sim 1 \text{ S/cm}$, [40, 41]) was attributed to the strong Coulomb interactions between the UV released electrons which migrate along a narrow conducting channel – the hopping path (Fig. 3). Alleviation of the electronic repulsion [42] resulted in the observed [44] 100-fold enhancement of the conductivity in the mayenite-based oxide, $[\text{Ca}_{12}\text{Al}_{14}\text{O}_{32}]^{2+}(2e^-)$, although the carrier concentration was only two times larger than that in the H-doped UV-irradiated $\text{Ca}_{12}\text{Al}_{14}\text{O}_{33}$. The improved conductivity, however, came at the cost of greatly increased absorption [42, 44] due to an increased density of states at the Fermi level, making this oxide unsuitable for practical use as a transparent conducting material.

Despite the failure to combine effectively the optical transparency with useful electrical conductivity in $\text{Ca}_{12}\text{Al}_{14}\text{O}_{33}$, the band structure analysis of the mayenite-

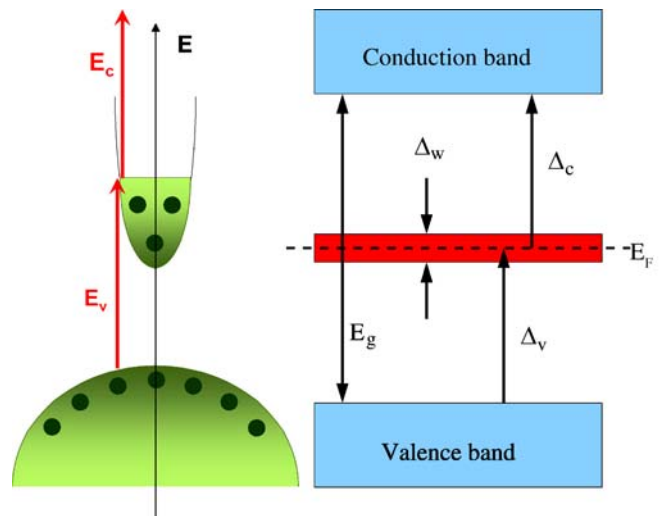


FIGURE 5 Schematic band structure of conventional (left) and “ideal” (right) transparent conductor

based oxides suggests that these materials belong to a conceptually new class of transparent conductors where a significant correlation between their structural peculiarities and electronic and optical properties allows achieving good conductivity without compromising their optical properties. In striking contrast to the conventional TCOs, where there is a trade-off between optical absorption and conductivity, as discussed above, nanoporous materials allow a possibility to combine 100% optical transparency with high electrical conductivity. The schematic band structure of such an “ideal” TCO is shown in Fig. 5. Introduction of a deep impurity band in the bandgap of an insulating material would help to keep intense interband transitions (from the valence band to the impurity band and from the impurity band to the conduction band) above the visible range. This requires the bandgap of a host material to be more than 6.2 eV . Furthermore, the impurity band should be narrow enough (less than 1.8 eV) to keep intraband transitions (as well as the plasma frequency) below the visible range.

In order to achieve high conductivity, the concentration of impurities should be large enough so that their electronic wavefunctions overlap and form an impurity band. The formation of the band would lead to a high carrier mobility due to the extended nature of these states resulting in a relatively low scattering. For this, a material with a close-packed structure should not be used, because large concentration of impurities would result in (1) an increase of ionized impurity scattering which limits electron transport; and (2) a large relaxation of the host material, affecting its electronic structure and, most likely, decreasing the desired optical transparency. Therefore,

² We employed highly precise all-electron full-potential linearized augmented plane wave (FLAPW) method [45, 46] with the local density approximation for the electronic band structure investigations of Mo-doped In_2O_3 , multicomponent XY_2O_4 compounds, H-doped $\text{Ca}_{12}\text{Al}_{14}\text{O}_{33}$ and oxygen deficient $[\text{Ca}_{12}\text{Al}_{14}\text{O}_{32}]^{2+}(2e^-)$. Each structure has been optimized via the total energy and atomic forces minimization. During the optimization, all atoms were allowed to move along x , y , and z directions while the lattice parameters were fixed at the corresponding experimental values. The UV-irradiated H-bearing $\text{Ca}_{12}\text{Al}_{14}\text{O}_{33}$ was investigated within the linear muffin-tin orbital method (LMTO) in the atomic sphere approximation [47].

an introduction of a deep impurity band into a wide-band insulator with a close-packed structure would make the material neither conducting nor transparent. Alternatively, materials with a nanoporous structure may offer a way to incorporate a large concentration of impurities without any significant changes in the band structure of the host material. Zeolites have been proposed [5] as potential candidates for the “ideal” TCOs because they possess the desired structural and optical features, i.e., spacious interconnected pores and large bandgaps, and exhibit the ability to trap functional “guest” atoms inside the nanosized cavities, which would govern the transport properties of the material.

Thus, understanding the principles of the conventional transparent conductors provides a solid base for further search of novel TCO host materials as well as efficient carrier generation mechanisms. Ab-initio density-functional band structure investigations² are valuable not only in providing a thorough insight into the TCO basics but also in predicting hidden capabilities of the materials beyond the traditionally employed.

REFERENCES

- 1 A.J. Freeman, K.R. Poeppelmeier, T.O. Mason, R.P.H. Chang, T.J. Marks, *Mater. Res. Soc. Bull.* **25**, 45 (2000)
- 2 O.N. Mryasov, A.J. Freeman, *Phys. Rev. B* **64**, 233 111 (2001)
- 3 R. Asahi, A. Wang, J.R. Babcock, N.L. Edleman, A.W. Metz, M.A. Lane, V.P. Dravid, C.R. Kannewurf, A.J. Freeman, T.J. Marks, *Thin Solid Films* **411**, 101 (2002)
- 4 H. Mizoguchi, P.M. Woodward, *Chem. Mater.* **16**, 5233 (2004)
- 5 J.E. Medvedeva, A.J. Freeman, *Europhys. Lett.* **69**, 583 (2005)
- 6 S. Jin, Y. Yang, J.E. Medvedeva, J.R. Ireland, A.W. Metz, J. Ni, C.R. Kannewurf, A.J. Freeman, T.J. Marks, *J. Am. Chem. Soc.* **126**, 13787 (2004)
- 7 Y. Yang, S. Jin, J.E. Medvedeva, J.R. Ireland, A.W. Metz, J. Ni, M.C. Hersam, A.J. Freeman, T.J. Marks, *J. Am. Chem. Soc.* **127**, 8796 (2005)
- 8 J.E. Medvedeva, *Phys. Rev. Lett.* **97**, 086401 (2006)
- 9 J.R. Bellingham, W.A. Phillips, C.J. Adkins, *J. Mater. Sci. Lett.* **11**, 263 (1992)
- 10 T.J. Coutts, D.L. Young, X. Li, *Mater. Res. Bull.* **25**, 58 (2000)
- 11 Y. Meng, X. Yang, H. Chen, J. Shen, Y. Jiang, Z. Zhang, Z. Hua, *Thin Solid Films* **394**, 219 (2001); *J. Vac. Sci. Technol. A* **20**, 288 (2002)
- 12 Y. Yoshida, T.A. Gessert, C.L. Perkins, T.J. Coutts, *J. Vac. Sci. Technol. A* **21**, 1092 (2003); C. Warmsingh, Y. Yoshida, D.W. Readey, C.W. Teplin, J.D. Perkins, P.A. Parilla, L.M. Gedvilas, B.M. Keyes, D.S. Ginley, *J. Appl. Phys.* **95**, 3831 (2004)
- 13 Y. Yoshida, D.M. Wood, T.A. Gessert, T.J. Coutts, *Appl. Phys. Lett.* **84**, 2097 (2004)
- 14 S. Sun, J. Huang, D. Lii, *J. Vac. Sci. Technol. A* **22**, 1235 (2004); S. Sun, J. Huang, D. Lii, *J. Mater. Res.*, **20**, 247 (2005)
- 15 I. Hamberg, C.G. Granqvist, K.F. Berggren, B.E. Sernelius, L. Engström, *Phys. Rev. B* **30**, 3240 (1984)
- 16 H. Kawazoe, N. Ueda, H. Un'no, T. Omata, H. Hosono, H. Tanoue, *J. Appl. Phys.* **76**, 7935 (1994)
- 17 M. Orita, M. Takeuchi, H. Sakai, H. Tanji, *Japan. J. Appl. Phys.* **34**, L1550 (1995)
- 18 M. Orita, H. Tanji, M. Mizuno, H. Adachi, T. Tanaka, *Phys. Rev. B* **61**, 1811 (2000)
- 19 H. Kaga, R. Asahi, T. Tani, *Japan. J. Appl. Phys.* **43**, 7133 (2004)
- 20 H. Hiramatsu, H. Ohta, W.S. Seo, K.J. Koumoto, *J. Japan. Soc. Powder Metall.* **44**, 44 (1997)
- 21 M. Orita, H. Ohta, M. Hirano, S. Narushima, H. Hosono, *Philos. Mag. B* **81**, 501 (2001)
- 22 K. Nomura, H. Ohta, K. Ueda, T. Kamiya, M. Hirano, H. Hosono, *Science* **300**, 1269 (2003)
- 23 K. Nomura, H. Ohta, A. Takagi, T. Kamiya, M. Hirano, H. Hosono, *Nature* **432**, 488 (2004)
- 24 A. Takagi, K. Nomura, H. Ohta, H. Yanagi, T. Kamiya, M. Hirano, H. Hosono, *Thin Solid Films* **486**, 38 (2005)
- 25 Von K. Kato, I. Kawada, N. Kimizuka, T. Katsura, *Z. Krist.* **141**, 314 (1975)
- 26 N. Kimizuka, T. Mohri, *J. Solid State Chem.* **60**, 382 (1985)
- 27 N. Kimizuka, T. Mohri, *J. Solid State Chem.* **78**, 98 (1989)
- 28 R.D. Shannon, J.L. Gillson, R.J. Bouchard, *J. Phys. Chem. Solids* **38**, 877 (1977)
- 29 H. Kawazoe, K. Ueda, *J. Am. Ceram. Soc.* **82**, 3330 (1999)
- 30 H. Kawazoe, H. Yanagi, K. Ueda, H. Hosono, *Mater. Res. Soc. Bull.* **25**, 28 (2000)
- 31 B.J. Ingram, G.B. Gonzalez, D.R. Kammler, M.I. Bertoni, T.O. Mason, *J. Electroceram.* **13**, 167 (2004)
- 32 J.E. Medvedeva, *Europhys. Lett.* (in press)
- 33 T. Minami, *J. Vac. Sci. Technol. A* **17**, 1765 (1999)
- 34 T. Minami, *Mater. Res. Soc. Bull.* **25**, 38 (2000)
- 35 T. Minami, *Semicond. Sci. Technol.* **20**, S35 (2005)
- 36 G.F. Neumark, *Mater. Sci. Eng. R* **21**, 1 (1997)
- 37 C.G. Van de Walle, *Phys. Stat. Solidi B* **229**, 221 (2002)
- 38 A. Zunger, *Appl. Phys. Lett.* **83**, 57 (2003)
- 39 C.G. Van de Walle, J. Neugebauer, *Nature* **423**, 626 (2003)
- 40 K. Hayashi, S. Matsuishi, T. Kamiya, M. Hirano, H. Hosono, *Nature* **419**, 462 (2002)
- 41 J.E. Medvedeva, A.J. Freeman, M.I. Bertoni, T.O. Mason, *Phys. Rev. Lett.* **93**, 16408 (2004)
- 42 J.E. Medvedeva, A.J. Freeman, *Appl. Phys. Lett.* **85**, 955 (2004)
- 43 M.I. Bertoni, T.O. Mason, J.E. Medvedeva, A.J. Freeman, K.R. Poeppelmeier, B. Delley, *J. Appl. Phys.* **97**, 103 713 (2005)
- 44 S. Matsuishi, Y. Toda, M. Miyakawa, K. Hayashi, T. Kamiya, M. Hirano, I. Tanaka, H. Hosono, *Science* **301**, 626 (2003)
- 45 E. Wimmer, H. Krakauer, M. Weinert, A.J. Freeman, *Phys. Rev. B* **24**, 864 (1981)
- 46 M. Weinert, E. Wimmer, A.J. Freeman, *Phys. Rev. B* **26**, 4571 (1982)
- 47 O.K. Andersen, O. Jepsen, M. Sob, M. Yussouff (eds.), *Electronic Band Structure and its Applications* (Springer, Berlin Heidelberg New York, 1986)